Body temperature measurement from the 17th century to the present days

Hindawi
Advances in Materials Science and Engineering
Volume 2019, Article ID 1241056, 10 pages
https://doi.org/10.1155/2019/1241056

Research Article

Effect of RE^{3+} on Structural Evolution of Rare-Earth Carbonates Synthesized by Facile Hydrothermal Treatment

Luca Spiridigliozzi,[1] **Grazia Accardo**,[2] **Domenico Frattini**,[3] **Antonello Marocco**,[1] **Serena Esposito**,[1] **Francesca S. Freyria**,[4,5] **Michele Pansini**,[1,5] **and Gianfranco Dell'Agli**[1,5]

[1]*Department of Civil and Mechanical Engineering, University of Cassino and Southern Lazio, Via G. Di Biasio 43, 03043 Cassino, FR, Italy*
[2]*Center for Hydrogen-Fuel Cell Research, KIST-Korea Institute of Science and Technology, Hwarang-ro 14-gil 5, Seongbuk-gu, Seoul, Republic of Korea*
[3]*Graduate School of Energy and Environment, Seoul National University of Science and Technology, 232 Gongneung-ro, Nowon-gu, Seoul, Republic of Korea*
[4]*Department of Applied Science and Technology, Politecnico di Torino, Corso Duca degli Abruzzi 24, Turin 10129, Italy*
[5]*INSTM-National Interuniversity Consortium of Materials Science and Technology, Via G. Giusti 9, 50121 Florence, Italy*

Correspondence should be addressed to Antonello Marocco; a.marocco@unicas.it

Received 12 November 2018; Revised 11 January 2019; Accepted 6 February 2019; Published 14 March 2019

Academic Editor: Peter Majewski

In this work, nanoparticles of cerium hydroxycarbonates were synthesized by a facile hydrothermal treatment at 120°C with ammonium carbonate as the precipitating/mineralizer agent in diluted solution. The as-formed amorphous coprecipitate undergoes several morphological and structural modifications as a function of the duration of the hydrothermal treatment, leading after 8 h to the formation of monosized nanoparticles of hexagonal $CeCO_3OH$. A similar behavior has been found when neodymium-based precursors are used as well, whereas the same treatment produces very different results by using different lanthanides-based precursors in terms of formed phases and morphologies, thus leading to the formation of pure tengerite-type structure phases, biphasic systems (tengerite type and hexagonal), or even entirely amorphous systems. Furthermore, the hydrothermal transformation is influenced by the redox behavior of the rare-earth cation (i.e., cerium) too, eventually resulting in the formation of fluorite-like structures. Therefore, a specific pathway of Ce(III) precursor transformations during hydrothermal treatment is proposed in this paper. Definitely, our results show that ammonium carbonate can be used as the precipitating/mineralizer agent to obtain cerium, doped-cerium, and neodymium hydroxycarbonates, which show excellent morphologies (i.e., characterized by spherical, nanosized particles with monomodal size distribution). Therefore, they can be used as optimal precursors for oxide powders. Conversely, when tengerite-type carbonate precursors are formed, their morphology is characterized by large and acicular particles.

1. Introduction

Rare-earth-based materials have drawn attention in the past years due to their wide range of applications, in the lighting industry [1], in electrochemical energy devices [2], in catalysis [3], and in biological [4] and magnetic [5] applications. Their very interesting properties are largely due to the unique 4f electron orbitals having highly localized electronic states and very predictable electronic transitions [6], weakly influenced by either the coordination environment or the crystal field. Among rare-earth materials, the rare-earth carbonates, both amorphous and crystalline, have recently attracted considerable research work to search for potential materials for specialized industrial applications [7].

As a further evidence of the great technological interest in this field, in the last few years, Kaczmarek et al. [8] and Kim et al. [9] authored two systematic reviews concerning rare-earth carbonates and hydroxycarbonates. At room temperature and pressure (25°C and 1 atm), the rare-earth carbonates are divided in two groups: the hydrated normal rare-earth carbonates ($RE_2(CO_3)_3{\cdot}xH_2O$) and the rare-earth hydroxycarbonates ($RE(OH)CO_3{\cdot}xH_2O$) [9]. Nowadays, these materials, beside their intrinsic properties, are also very appealing for their potential as precursors for nano- and microsized rare-earth oxides [8, 10].

In recent scientific literature, various synthesis methods have been proposed to produce different rare-earth carbonates, and among them, the most common ones are precipitation [11] and homogeneous precipitation [12, 13], sonochemical synthesis [14], and hydrothermal treatment [15, 16]. In particular, the latter can be considered an effective and cheap route, thanks to low synthesis temperature, high powder reactivity, and shape control [17, 18], and therefore, it can be frequently used for large-scale production [8]. Indeed, the hydrothermal technique has been becoming one of the most important tools for advanced ceramic processing, particularly in nanostructured materials applications, mainly because it is easy to obtain monodispersed and highly homogeneous nanocrystals [19].

Among the rare-earth carbonates, cerium-based carbonates account for a prominent role, and several reports can be found in literature about the hydrothermal synthesis of cerium carbonates. For example, Nakagawa et al. [20] obtained spherical nanoparticles of hexagonal CeO_3OH treated at 140°C for 96 h and cerium oxycarbonate particles with different morphologies by adding laurylamine in the mineralizer solution; Sun et al. [21] synthesized flower-like particles of mixed orthorhombic and hexagonal $CeOHCO_3$ at 180°C for 72 h; and Hrizi et al. [22] obtained various morphologies of orthorhombic $CeOHCO_3$ by varying the cetyltrimethylammonium bromide/Ce ratio in systems formed by $Ce(NO_3)_3$ and urea treated at 180°C for 3 h. On the contrary, Han et al. [23] reported that, by hydrothermal treatments below 150°C, amorphous or poorly crystallized cerium carbonate powders are obtained. Thus, very different results starting from hydrothermal treatments have been reported in terms of formed phases and morphologies, depending on temperature and duration of the hydrothermal method and mineralizer solution composition.

The aim of the present work is to synthesize, via a facile hydrothermal treatment, rare-earth carbonate-based nanopowders to be used as precursors for oxide powders characterized by very good sinterability after a mild calcination step. Focusing on many potential practical applications, the adopted hydrothermal process was kept as simple and cheap as possible, i.e., by applying low temperature (120°C), by using cheap raw materials without any additives. Finally, the work was mainly hinged on the hydrothermal synthesis of cerium carbonate-based materials and on finding the optimal synthesis conditions to produce them. In addition, the same hydrothermal conditions were also applied by using other rare-earth precursors to study their influence on both structure and microstructure of the formed phases.

Our results show that the hydrothermal transformations of cerium compounds are rather complex, involving several phases evolution before achieving an equilibrium state. Furthermore, significant differences emerge for samples containing different rare-earth compounds, in terms of both phases and morphologies, probably due to the lanthanides contraction law. Finally, some recipes for preparing rare-earth carbonate-based powders via facile hydrothermal synthesis are proposed.

2. Materials and Methods

Cerium(III) nitrate ($Ce(NO_3)_3{\cdot}6H_2O$ 99.0% Sigma-Aldrich, Italy) as the cerium precursor and ammonium carbonate ($(NH_4)_2CO_3$ with $NH_3 > 30\%$ Fluka, Italy) as the precipitating/mineralizing agent were used as starting chemicals for the hydrothermal syntheses. For the other rare-earth-based materials, the corresponding hydrated nitrates (i.e., $RE(NO_3)_3{\cdot}xH_2O$ 99.9% from Sigma Aldrich, Italy, $x = 5$ or 6, depending on different rare-earth precursors) were used. All the chemicals were used as-received without any further purification.

Independently of the final composition, the procedure for the hydrothermal syntheses was the following:

(a) A proper amount of rare-earth nitrate was dissolved in deionized water to obtain a 0.1 M solution (solution A), and ammonium carbonate was dissolved in deionized water up to 0.5 M (solution B). Both solutions were vigorously stirred for 1 h to favor the homogenization.

(b) A proper volume of solution B was quickly added to the selected volume of solution A, maintained under mild stirring, in order to reach $R = 2.5$, where R is the molar ratio between carbonate ions and total metal cations. Some experiments were also carried out at $R = 10$. When the solution B was quickly added to solution A, a white precipitate was instantly formed.

(c) The as-prepared suspensions were transferred in Teflon vessels (60 mL), which were then sealed and held in outer stainless steel pressure vessels for the hydrothermal treatment. The treatment was carried out in an air-thermostated rotating oven at 120°C and 25 rpm to allow the complete homogenization of the system during the process.

(d) After the selected reaction times, the vessels were quenched with cold water, and the resulting products were repeatedly filtered by using a vacuum pump, washed with distilled deionized water, and finally dried overnight at 80°C in static air. The various synthesized samples and their labels are reported in Table 1.

All samples were characterized by X-ray powder diffraction (XRD) using a Panalytical X'PERT MPD diffractometer to detect the crystalline phases. The primary crystallite size was calculated by the Scherrer equation [24]:

Table 1: Synthesized samples and synthesis conditions.

Sample	Used rare earths	Duration (h)	R ratio (–)
C0	Ce^{3+}	0	2.5
C1	Ce^{3+}	1	2.5
C2	Ce^{3+}	2	2.5
C4	Ce^{3+}	4	2.5
C8	Ce^{3+}	8	2.5
C16	Ce^{3+}	16	2.5
C48	Ce^{3+}	48	2.5
C168	Ce^{3+}	168	2.5
N16	Nd^{3+}	16	2.5
S16	Sm^{3+}	16	2.5
G16	Gd^{3+}	16	2.5
D16	Dy^{3+}	16	2.5
H16	Ho^{3+}	16	2.5
E16	Er^{3+}	16	2.5
Y16	Yb^{3+}	16	2.5
SC16	$0.2Sm^{3+}$–$0.8Ce^{3+}$	16	2.5
C4-R10	Ce^{3+}	4	10
SC4-R10	$0.2Sm^{3+}$–$0.8Ce^{3+}$	4	10

$$d = \frac{K\lambda}{B\cos(\theta)}, \tag{1}$$

where K is the shape factor equal to 0.89 for spherical particles, λ is the X-ray wavelength (0.1541 nm for Cu Kα_1), θ is the Bragg's angle of the peak, and B is the relative full width at half maximum (FWHM) corrected for the instrumental broadening. B is calculated as

$$B = B_{\text{sample}} - B_{\text{instr}}, \tag{2}$$

where B_{instr} is determined using standard polycrystalline silicon. Both fitting profiles were made using the pseudo-Voigt function as a mathematical model for the XRD peaks, and the calculations related to the Scherrer formula were carried out using the software X'Pert HighScore from Panalytical. The quantitative phase analysis was performed according to the method recently proposed by Toraya [25], whereas the calculations to extract the integrated intensities of the XRD peaks (up to 60°·2θ) were carried out by using the software X'Pert HighScore from Panalytical.

The specific surface area was measured by the nitrogen adsorption/desorption isotherms technique through the Brunauer–Emmett–Teller (BET) method using a Micromeritics Gemini apparatus; before the measurement, the sample was preliminary degassed under vacuum at 100°C.

The thermal behavior of the samples was investigated through simultaneous differential scanning calorimetry and thermogravimetric analysis (DSC and TGA, Thermal analyzer STA 409, Netzsch) in air, with a heating rate of 10°C/min up to 1200°C; α-Al_2O_3 was used as a reference.

The morphology of the powders was observed by scanning electron microscopy (SEM) (Inspect F, FEI Co., USA).

3. Results and Discussion

During hydrothermal synthesis, different routes of crystallization of the samples were observed, and the phases obtained and their evolution are mostly driven by the selected rare-earth cation. Firstly, the cerium-based precipitate is mainly amorphous, as clearly evident from its diffraction pattern (Figure 1(a)), thus confirming the well-known results reported elsewhere [7, 10], in which amorphous precipitates are formed from a supersaturated aqueous solution containing rare-earth cations and carbonate ions at $R = 2.5$. Being amorphous, a univocal phase identification by diffraction analysis is not possible; however, the thermogravimetric analysis (Figure 1(b)) along with analogous results reported in [10, 11] allows supposing that it is constituted by a hydroxycarbonate ($CeCO_3OH$). In fact, it is possible to exclude the normal cerium carbonate, whose minimal weight loss should be more than 25%, whereas the thermal decomposition of cerium hydroxycarbonate is expected to be 20.7% weight loss, according to the following reaction:

$$(\text{amorphous}) - CeCO_3OH + \frac{1}{4}O_2 \longrightarrow CeO_2 + CO_2 + \frac{1}{2}H_2O. \tag{3}$$

Therefore, our measured weight loss (i.e., 21%, Figure 1(b)) is in very good agreement with the theoretical one. The amorphous precipitate, instantly formed when solution B is added to solution A, might be obtained by the following two-step reactions, considering that the hydrated Ce^{3+} cation can undergo hydrolysis in aqueous solution, as also proposed by Hirano and Kato [26]:

$$\left[Ce(H_2O)_n\right]^{3+} + H_2O \longleftrightarrow \left[CeOH(H_2O)_{n-1}\right]^{2+} + H_3O^+, \tag{4}$$

$$\left[CeOH(H_2O)_{n-1}\right]^{2+} + {CO_3}^{2-} \longrightarrow (\text{amorphous}) - CeCO_3OH + (n-1)H_2O. \tag{5}$$

During the hydrothermal treatment, the amorphous precipitate undergoes several phase transformations. The diffraction patterns of C samples, treated up to 168 h for different times, are shown in Figure 2, clearly suggesting the crystallization route during the ongoing hydrothermal treatment. After 1 h, the sample is still essentially amorphous, although several very small and broad peaks of orthorhombic $CeCO_3OH$ (ICDD card no. 41-0013) begin to appear (Figure 2(a)), thus indicating the onset of the hydrothermal crystallization of the amorphous precipitate. This transformation occurring very likely through a dissolution-crystallization mechanism is favored by the higher solubility of the amorphous precursors with respect to the crystalline phases. After 2 h (Figure 2(b)), the crystallization process continues, and in addition to orthorhombic $CeCO_3OH$ (which is the main crystalline phase), the hexagonal $CeCO_3OH$ phase begins to form, as showed by some small and broad XRD peaks attributable to this phase (ICDD card no. 62-0031). By extending the hydrothermal process up to 8 h (Figure 2(d)), the amount of the hexagonal phase increases (Figure 2(c)). At longer times, the orthorhombic phase is not present anymore, being the

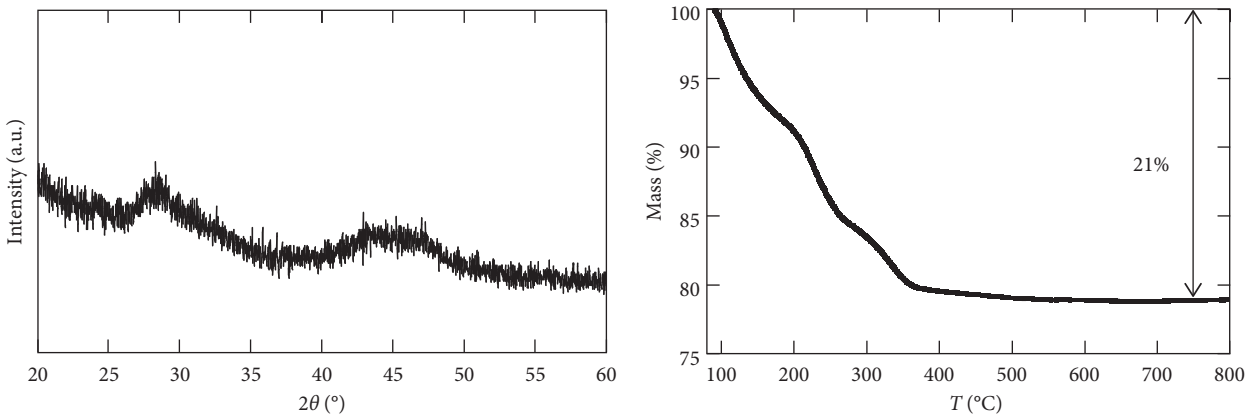

Figure 1: X-ray diffraction pattern (a) and thermogravimetric plot (b) of cerium-based precipitate, i.e., sample C0.

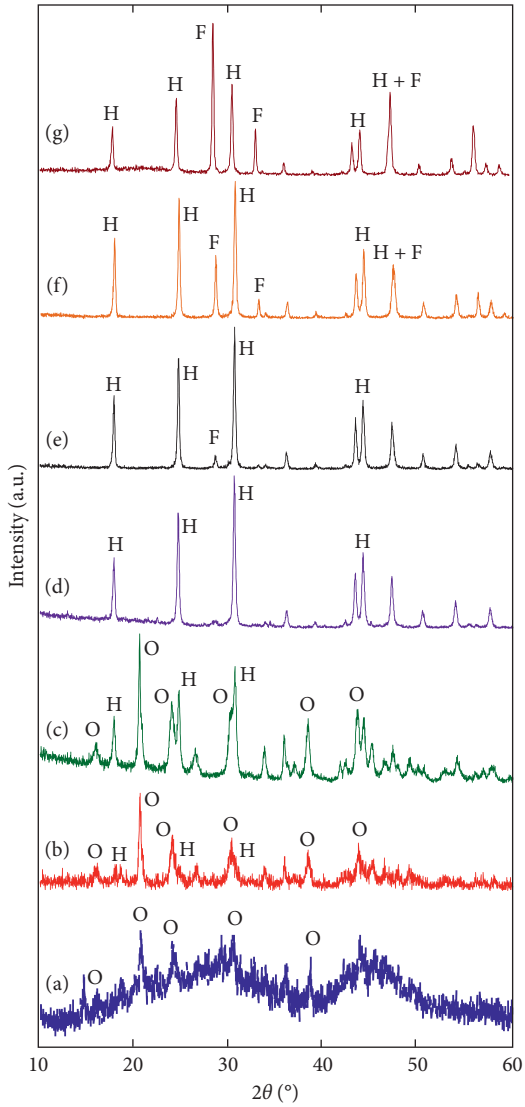

Figure 2: Diffraction patterns of hydrothermally treated cerium-based samples: C1 (a); C2 (b); C4 (c); C8 (d); C16 (e); C48 (f); C168 (g). The main XRD peaks are labelled with O for orthorhombic $CeCO_3OH$, H for hexagonal $CeCO_3OH$, and F for fluorite-type structure CeO_2.

sample constituted only by hexagonal $CeCO_3OH$. These findings suggest that the orthorhombic polymorphic form is the first one to crystallize and it is indeed a metastable phase, easily converted into the hexagonal one. This is not surprising because in the hydrothermal process, metastable phases are often firstly formed [27]. However, after the formation of the hexagonal phase, the system has not still achieved the equilibrium state. The redox behavior of cerium cations can induce further transformations as long as the oxidizing conditions are preserved during the treatment, i.e., sufficient O_2 is present in the system. In fact, by a careful inspection of Figure 2(e) (related to 16 h of process), the main XRD peaks of cerianite (CeO_2, ICDD card no. 75-390) distinctly appear. The Ce^{3+} oxidation with the consequent formation of cerianite is not surprisingly a slow transformation, requiring many hours, especially at the low adopted temperature. Several steps are involved in this transformation (oxidation of Ce^{3+}, evolution of CO_2 and H_2O, breakdown of hexagonal lattice, and formation of fluorite lattice) which can be generally represented by the following chemical reaction:

$$h - CeCO_3OH + \frac{1}{4}O_2 \longrightarrow CeO_2 + CO_2 + \frac{1}{2}H_2O. \quad (6)$$

It is worth mentioning that even though equation (3) seems similar to equation (6), they are completely different. In fact, the former one occurs in dried powders and it is induced by the temperature during the TGA analysis (Figure 1(b)); on the contrary, the latter one occurs during the hydrothermal treatment at 120°C between the solid dispersed in the mineralizer solution and the O_2 dissolved in it.

By comparing the diffraction patterns of samples C48 (Figure 2(f)) and C168 (Figure 2(g)), we can note that the intensity of XRD peaks of cerianite increases and the one of XRD peaks of the hexagonal phase decreases. The estimation of both cerianite and hexagonal phase amounts in samples C48 and C168 was carried out through the method recently proposed by Toraya [25], using all the peaks up to 60° 2θ. On the basis of this procedure, cerianite is 19.1% w/w in sample C48 and 46.8% w/w in sample C168. Therefore, by increasing the duration of the synthesis method, the transformation of equation (6) keeps going on, and after 48 h

(Figure 2(f)) and 168 h (Figure 2(g)), the amount of cerianite is significantly increased (i.e., more than doubled). To this regard, it should also be noted that the complete transformation of $CeCO_3OH$ in CeO_2 requires an amount of O_2 which is probably not present in the small reactors used in our experiments. Anyway, it is clearly evident that the oxidation of Ce^{3+} to Ce^{4+} destabilizes the hexagonal hydroxycarbonate, conversely favoring the formation of the fluorite-structured CeO_2. As long as a sufficient duration of the treatment is guaranteed (and an adequate oxidizing condition is maintained, i.e., the available O_2 in the closed system is sufficient to oxidize all Ce^{3+} cations), the stable phase of hydrothermal ageing of Ce(III) nitrate in the presence of ammonium carbonate as the mineralizing/precipitating agent is indeed cerianite. However, the conversion into cerianite seems rationally rather weak at 120°C, even if an increase in the operating temperature could accelerate reaction (4). In this way, the formation of fluorite-structured ceria with a very good morphology could be directly obtained via hydrothermal synthesis. Moreover, an interest towards the cerium hydroxycarbonate should lead to select a proper duration of the hydrothermal treatment, i.e., 8 h by adopting our chemical-physical conditions.

These phase transformations proceed with the corresponding morphological modifications of the powders. In Figure 3, some exemplary SEM micrographs of the samples are reported. Sample C0, i.e., the as-obtained amorphous precipitate, is constituted by relatively large agglomerates of irregular particles without a well-defined shape. These agglomerates are gradually broken during the hydrothermal process, completely disappearing after 8 h (Figure 3(e)). Clearly, this morphological evolution can be explained only by supposing a dissolution-reprecipitation (crystallization) mechanism, thus confirming previous data reported in literature [11]. During the fragmentation and dissolution of the agglomerates, some particles emerge from them, as well visible in Figures 3(b), 3(c), and 3(d), in which both elongated particles and spherical-like particles can be noticed. As the former ones are firstly obtained, they are very probably constituted by orthorhombic $CeCO_3OH$, especially by considering Figure 2(a) and Nakagawa et al. results in [20], in which orthorhombic $CeCO_3OH$ particles show a shuttle-like (i.e., elongated) morphology. On the contrary, the spherical-like particles are reasonably constituted by hexagonal $CeCO_3OH$, as sample C8 is constituted only by this phase (Figure 2(d)), showing a very homogeneous microstructure (Figure 3(e)) characterized by rounded particles whose average size is about 100 nm. This value is also consistent with the crystallite size of 60 nm calculated by using the Scherrer formula on the peak (302) at 30.50° 2θ. Therefore, through our facile 8-hour hydrothermal treatment, monophasic hexagonal $CeCO_3OH$ powders characterized by an excellent morphology, nanometer size with monomodal distribution, were synthesized.

Extending the hydrothermal treatment longer than 8 h did not cause any relevant morphological evolution, and the homogeneous microstructure of spherical-like particles is maintained up to 168 h (Figures 3(f), 3(g), and 3(h)). Cerianite is practically negligible in C16, whilst it is 19.1% w/w in C48 and 46.8% w/w in C168, and the reaction (6) occurring during the hydrothermal process takes place without morphological modifications, thus leading to exclude a dissolution-precipitation mechanism for equation (6). As a confirmation of that, a careful inspection on Figures 3(f), 3(g), and 3(h) reveals that particles size is roughly unaltered. This evidence is further confirmed by the calculated crystallite size of the corresponding samples: 65 nm for the hexagonal $CeCO_3OH$ of samples C16, C48, and C168 and 85 nm for the cubic CeO_2 of samples C48 and C168 (in sample C16, the (111) peak of cubic CeO_2 is too weak to calculate the crystal size by Scherrer formula). Those values are consistent with the measured surface area too. In fact, the C168 surface area is 11 m^2/g, corresponding to approx. 100 nm as the average diameter, under the hypothesis that the contents of cubic CeO_2 and hexagonal $CeCO_3OH$ are 46.8% w/w and 53.2% w/w, respectively.

In conclusion, based on the obtained results, we can suggest that the following sequence of transformations occurs to the cerium carbonate precursor upon the hydrothermal treatment with ammonium carbonate as the precipitating/mineralizing agent:

$$\text{amorphous} - CeCO_3OH \longrightarrow o - CeCO_3OH \cdot (\text{fast transformation}), \tag{7}$$

$$o - CeCO_3OH \longrightarrow h - CeCO_3OH \cdot (\text{fast transformation}), \tag{8}$$

$$h - CeCO_3OH + \frac{1}{4}O_2 \longrightarrow CeO_2 + CO_2 + \frac{1}{2}H_2O \cdot (\text{slow transformation}). \tag{9}$$

The proposed rates of the transformation (7), (8), and (9) are obviously written in relative terms. In fact, based on the diffraction patterns in Figure 2, reactions (7) and (8) are completed within 8 h (very likely, the former is actually completed within 4 h), whereas reaction (6) requires a duration certainly higher than 48 h. As reported above, cerianite content in C48 is less than 20% w/w, which will increase significantly as the hydrothermal treatment proceeds. We can also suppose that the fast transformations (7) and (8) are based on a dissolution-reprecipitation mechanism, as the morphology of the powder is completely changed after them, whereas, the slow transformation (9) does not proceed via a dissolution-reprecipitation mechanism as before mentioned; therefore, another mechanism should be invoked.

From this background, many different rare-earth carbonates were synthetized in the same hydrothermal conditions (i.e., 16 h at 120°C). The selected duration is a little higher than the one needed for the hexagonal $CeCO_3OH$ to be formed, mainly because of the absence of multiple oxidation states in the other used lanthanides preventing a transformation like equation (9). Therefore, a higher treatment duration could favor the completion of the hydrothermal transformations.

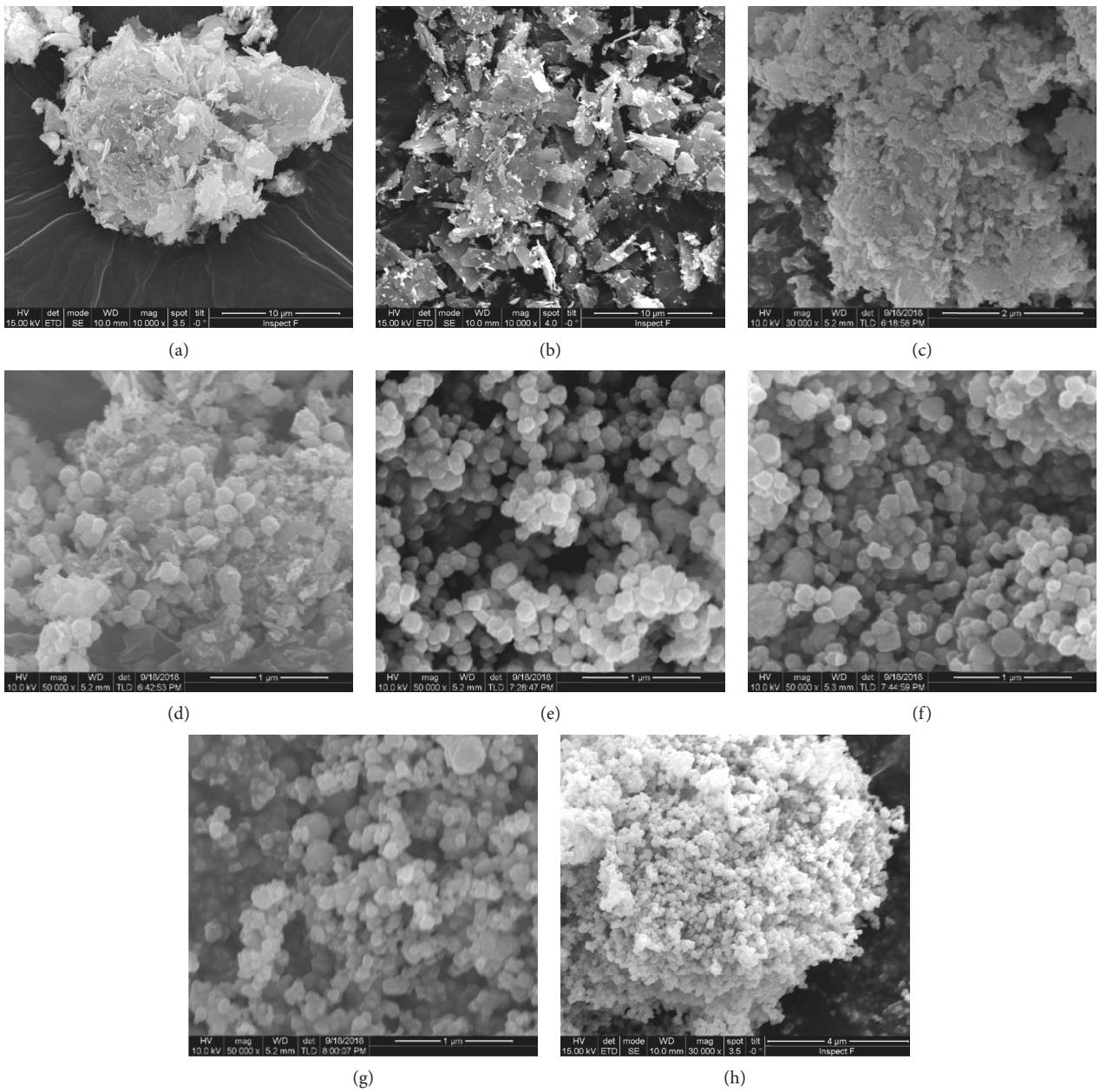

Figure 3: SEM micrographs of selected hydrothermally treated cerium-based samples: (a) C0; (b) C1; (c) C2; (d) C4; (e) C8; (f) C16; (g) C48; (h) C168.

In Figures 4(a) (rare earths with lower atomic number) and Figure 4(b) (rare earths with higher atomic number), the diffraction patterns of all samples treated for 16 h are displayed. By analyzing samples G16, D16, H16, and E16 (Figures 4(b)), we can notice that all these samples exhibit the same diffraction pattern, even if a progressive shift in the peaks position is clearly evident, as reported in the inset of Figures 4(b), showing a magnification of the most intense peak located in the range 11.5–12°·2θ. To the best of our knowledge, in the ICDD database, there are no cards containing Gd or Dy or Ho or Er characterized by the same diffraction patterns as those in Figures 4(b). Anyway, all their peaks can be attributed to ICDD card no. 81-1538, corresponding to $Y_2(CO_3)_3{\cdot}2H_2O$, a compound known as Y-tengerite with the orthorhombic crystal structure (despite the abovementioned progressive shift in peaks position). Therefore, the corresponding phase shown in Figure 4(E) can be identified as $Gd_2(CO_3)_3{\cdot}2H_2O$, isostructural to Y-tengerite. Analogous chemical formulas can be used for Dy, Ho, and Er, showing identical diffraction patterns. Therefore, samples G16, D16, H16, and E16 are all monophasic, tengerite-type, i.e., hydrated, rare-earth carbonates with an orthorhombic crystal structure. This conclusion also agrees with the general knowledge that rare-earth carbonates from samarium through thulium (plus yttrium) are isostructural to tengerite [9]. Moreover, the shifts highlighted in the inset of Figures 4(b) are in perfect agreement with the contraction law of lanthanides. In fact, the ionic radius

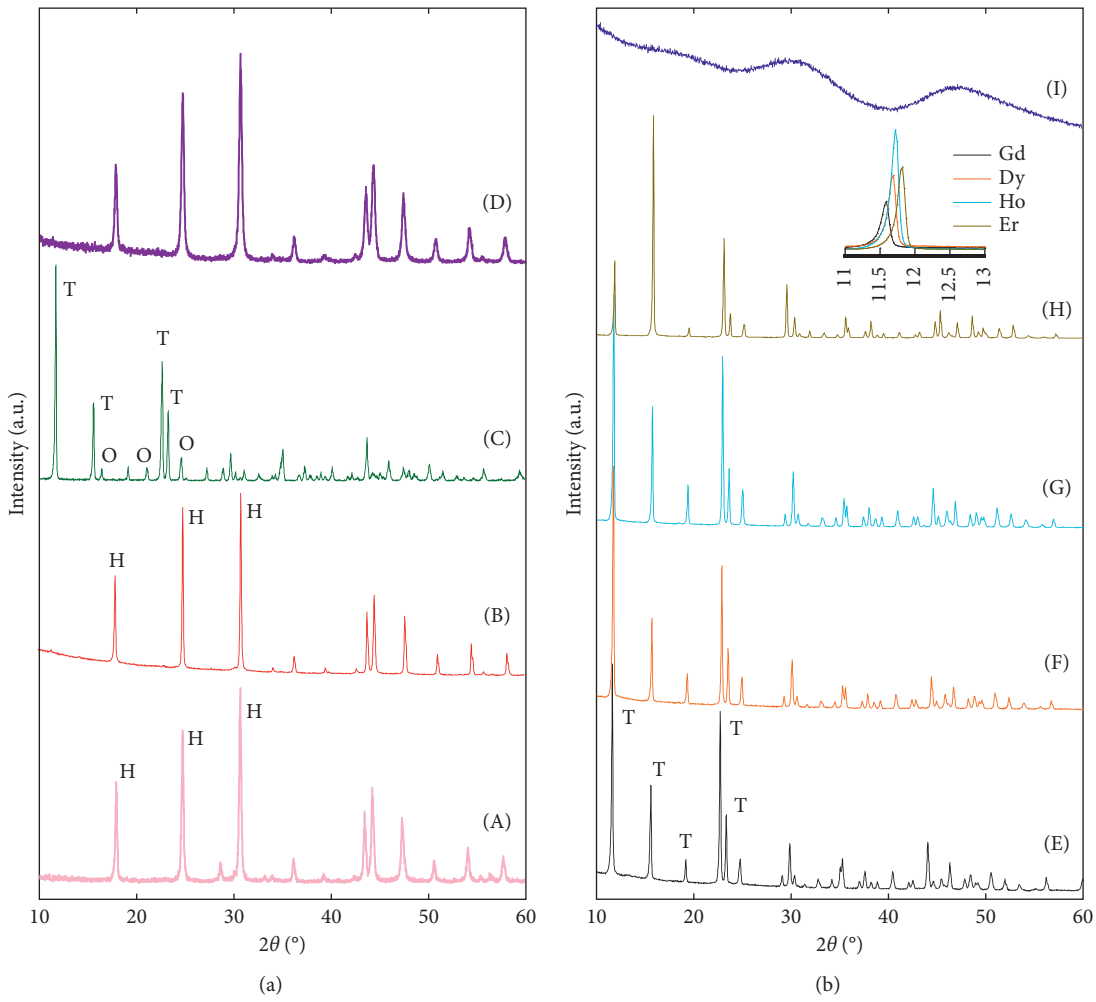

Figure 4: Diffraction patterns of samples hydrothermally treated for 16 h. (a) Rare earths with a lower atomic number: Ce-based sample (A); Nd-based sample (B); Sm-based sample (C); Sm- (20%-) cerium- (80%-) based sample (D). (b) Rare earths with a higher atomic number: Gd-based sample (E), Dy-based sample (F), Ho-based sample (G), Er-based sample (H), and Yb-based sample (I). The inset reports a magnification of the most intense XRD peak of the tengerite-type structure present in different samples. The main XRD peaks are labelled with H for hexagonal $RECO_3OH$, O for orthorhombic $RECO_3OH$, and *T* for the tengerite-type $RE_2(CO_3)_3{\cdot}2H_2O$.

continuously decreases from Gd^{3+} to Er^{3+} (from 0.1053 nm to 0.1004 nm, respectively), with a consequent decrease of the interatomic distances and, in turn, an increase of the Bragg angles.

On the contrary, by using Yb as rare earth, no sign of crystallization occurred after 16 h of hydrothermal treatment, as shown in Figure 4(H). A deeper study to unravel the conditions to hydrothermally induce Yb-based precursors crystallization was outside the scope of this work, and no further investigation was carried out.

In Figure 4(a), the diffraction patterns of samples C16, N16, S16, and CS16 are reported. Sample N16 (Figure 4(B)) exhibits the same behavior of C16 (as above described). In fact, all its XRD peaks can be assigned to the hexagonal $NdCO_3OH$ (ICDD card no. 27-1295) which is isostructural to the cerium-based hexagonal phase. However, even if sample S16 is crystallized as well, its diffraction pattern (Figure 4(C)) appears much more complex compared to the other ones. By carefully inspecting Figure 4(C), we can identify the presence of all the main peaks of the already mentioned tengerite-type phase (marked with a "*T*"). Therefore, one of the first phase formed via hydrothermal treatment for Sm precursors seems to be an orthorhombic $Sm_2(CO_3)_3{\cdot}2H_2O$. Yet, in sample S16 at least a second crystalline phase is present, even if a direct identification of these Sm-based compounds has not been possible by consulting the ICDD database. However, by extending the research to a generic rare-earth element, we reasonably suppose that the additional phase could be the orthorhombic $SmCO_3OH$, isostructural to the orthorhombic $NdCO_3OH$ (ICDD card no. 27-1296). Actually, an orthorhombic $SmCO_3OH$ is present in the ICDD database (ICDD card no. 41-663), albeit exhibiting poor quality (even lacking of the space group) and not corresponding to S16 peak positions. Definitely, we can assume that, after 16 h of hydrothermal treatment, the Sm-based precursor is constituted by hydrated samarium carbonate and samarium hydroxycarbonate.

Finally, since Ce and Sm have shown a very different behavior, a further hydrothermal treatment under the same synthesis conditions was carried out on a system formed by

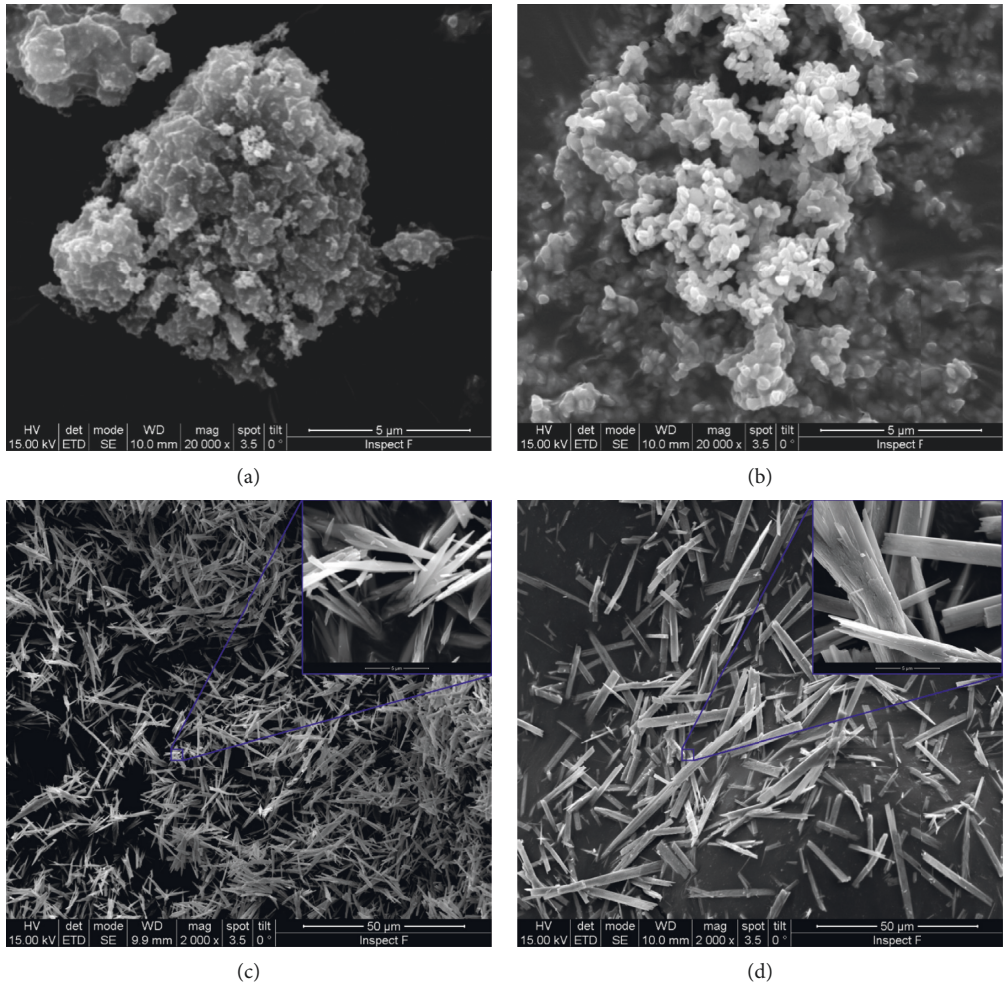

Figure 5: SEM micrographs of samples (a) Y16, (b) N16, (c) G16, and (d) E16.

20 mol% of Sm^{3+} and 80 mol% of Ce^{3+}. This particular composition has been also selected by considering that Sm-doped ceria has great importance as ceramic electrolyte for IT-SOFC. The corresponding diffraction pattern is reported in Figure 4(D), showing the presence of hexagonal $CeCO_3OH$ (possible composition is $Sm_{0.20}Ce_{0.80}CO_3OH$). It is interesting to notice that XRD peaks belonging to a fluorite-like structure do not appear in Figure 4(D) with respect to Figure 2(e), where almost 20% w/w of cerianite was already formed under the same treatment duration. Clearly, the presence of Sm in the lattice of hexagonal $CeCO_3OH$ makes the oxidation of Ce^{3+} and the simultaneous formation of the cubic CeO_2 more difficult, even if this transformation could start by prolonging the hydrothermal treatment duration.

Sample's morphology was revealed by SEM analysis, and four exemplary micrographs of samples treated for 16 h are shown in Figure 5. The morphology of the amorphous ytterbium-based compound (Figure 5(a)) is not well defined, similarly to the amorphous cerium-based compound. Sample N16 show small rounded particles in submicrometer assembled in clusters. The sharp shape of the XRD peaks in Figure 4(B) accounts for relatively large crystalline grains, whose size (calculated by the Scherrer formula) is 295 nm. This value is consistent with the particles shown in Figure 5(b). In this case, a dissolution-reprecipitation mechanism is involved to convert the as-synthesized amorphous precursors into a crystalline phase. Figure 5 also reports the tengerite-type phase morphology, related to samples G16 and E16, showing particles with a similar shape to the other samples. The dramatic difference of particles shape of G16 and E16 compared to the lanthanides with lower atomic number stands immediately out. Their morphology appears well homogeneous and characterized by acicular needle-like crystals of the tengerite type whose length is of some tenths of microns. A very similar morphology of the tengerite-type crystal was also recently reported in [7, 28] for hydrothermal treatments of rare-earth-based precursors.

Summarizing all the obtained results, it can be pointed out that

(i) rare earths with low atomic number (i.e., Ce and Nd) form hexagonal hydroxycarbonates with spherical, monomodal, and nanosized particles

(ii) intermediate-size rare earths (i.e., Sm) form biphasic products, i.e., orthorhombic hydroxycarbonate and tengerite type

(iii) rare earths with higher atomic number (i.e., Gd, Dy, Ho, and Er) form tengerite-type phases with elongated microsized particles

Therefore, the contraction law of lanthanides is again confirmed, as the rare-earth ionic radius heavily influences the formed phases and their consequent morphology.

In order to accelerate the hydrothermal crystallization, some additional experiments were conducted by using cerium and samarium-doped cerium precursors at the same temperature (120°C), for various duration, in the presence of a more concentrated mineralizer solution, as suggested in literature [29] as well. An R ratio value of 10 was selected for these experiments. Figure 6 shows the diffraction patterns of Ce- and of Sm-doped Ce treated for 4 h. It appears clearly that, with higher concentration of carbonate ions, the crystallization route is completely different, confirming the results reported in [16]. In fact, in Figure 6(a), a dissimilar and more complex diffraction pattern appears with respect to the one in Figure 2(c), relative to the same sample and treated for the same duration, in which in addition to the two phases detected in Figure 2(c), at least another crystalline phase appears; furthermore, the diffraction pattern in Figure 6(b) is even more complex. As a consequence, also the morphologies of samples in Figure 6 are affected by that.

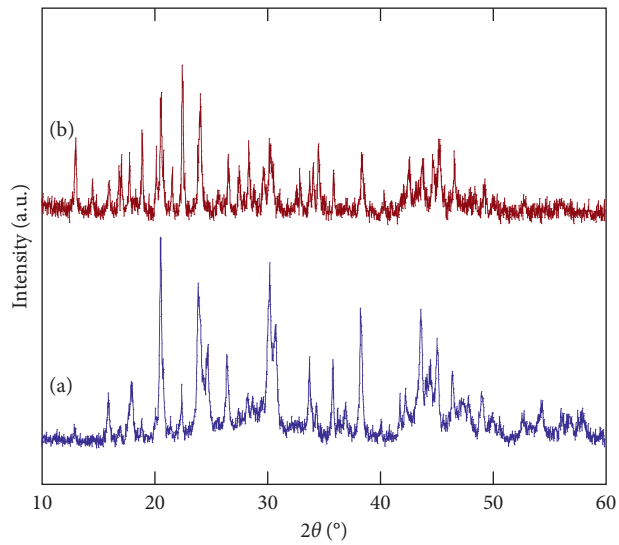

Figure 6: Diffraction patterns of the samples C4-R10 (a) and SC4-R10 (b) hydrothermally treated for 4 h at 120°C.

4. Conclusions

We found that the phase and morphology of rare-earth carbonates, hydrothermally synthesized at 120°C and in the presence of ammonium carbonate with $R = 2.5$, are strongly affected by the type of rare-earth precursors. A first, possible explanation is related to the multivalent behavior of some rare-earth elements. In the case of Ce and Nd, i.e., lanthanides with a lower atomic number, the formed phase is the hexagonal $RECO_3OH$ (if a proper duration of the hydrothermal treatment is used). In the case of Gd, Dy, Ho, and Er, i.e., lanthanides with a higher atomic number, hydrothermally treated for 16 h, the products are completely crystallized although the formed phase (i.e., the normal carbonate $RE_2(CO_3)_3{\cdot}2H_2O$ with the tengerite-type structure) and the morphology are completely different. In the case of Sm, i.e., a rare earth with an intermediate atomic number, a mixture of two crystalline phases is formed, i.e., the normal carbonate with the tengerite-type structure and the orthorhombic hydroxycarbonate. Finally, in the case of Yb, the analyzed rare earth with the highest atomic number, an amorphous product is obtained. This very different behavior is likely related to the contraction law of lanthanides. Since the most desired shape for practical applications is spherical-like particles from hexagonal $RECO_3OH$ (RE = Ce-, Nd-, and Sm-doped Ce), the tailored hydrothermal treatment designed in this work has been conducted at 120°C by using $(NH_4)_2CO_3$ as the precipitating/mineralizing agent, $R = 2.5$, and a duration between 8 and 16 h. Therefore, the use of a higher ratio R, i.e., a higher CO_3^{-2} concentration, or shorter times, is strongly counterproductive. The oxidation of the RE^{3+} cation, i.e., in the case of Ce, is possible at very long times (one week or more) and in the presence of O_2, which can cause the breakdown of the hexagonal lattice of the hydroxycarbonate with consequent formation of a fluorite-type lattice although this route is not practical and economically feasible.

Data Availability

The data used to support the findings of this study are available from the corresponding author upon request.

Conflicts of Interest

The authors declare that they have no conflicts of interest.

Acknowledgments

Dr. Grazia Accardo was supported by the Korea Research Fellowship Program, through the National Research Foundation of Korea (NRF) funded by the Ministry of Science and ICT (Grant no. 2016H1D3A1908428).

References

[1] L. Armelao, S. Quici, F. Barigelletti et al., "Design of luminescent lanthanide complexes: from molecules to highly efficient photo-emitting materials," *Coordination Chemistry Reviews*, vol. 254, no. 5-6, pp. 487–505, 2010.

[2] V. Esposito and E. Traversa, "Design of electroceramics for solid oxides fuel cell applications: playing with ceria," *Journal of the American Ceramic Society*, vol. 91, no. 4, pp. 1037–1051, 2008.

[3] H. He, H. Ma, D. Sun, L. Zhang, R. Wang, and D. Sun, "Porous lanthanide–organic frameworks: control over interpenetration, gas adsorption, and catalyst properties," *Crystal Growth & Design*, vol. 13, no. 7, pp. 3154–3161, 2013.

[4] C. Li and J. Lin, "Rare earth fluoride nano-/microcrystals: synthesis, surface modification and application," *Journal of Materials Chemistry*, vol. 20, no. 33, pp. 6831–6847, 2010.

[5] A. R. Chakhmouradian and F. Wall, "Rare earth elements: minerals, mines, magnets (and more)," *Elements*, vol. 8, no. 5, pp. 333–340, 2012.

[6] G. Accardo, D. Frattini, H. C. Ham, J. H. Han, and S. P. Yoon, "Improved microstructure and sintering temperature of bismuth nano-doped GDC powders synthesized by direct sol-gel combustion," *Ceramics International*, vol. 44, no. 4, pp. 3800–3809, 2018.

[7] B. Vallina, J. D. Rodriguez-Blanco, A. P. Brown, J. A. Blanco, and L. G. Benning, "The role of amorphous precursors in the crystallization of La and Nd carbonates," *Nanoscale*, vol. 7, no. 28, pp. 12166–12179, 2015.

[8] A. M. Kaczmarek, K. Van Hecke, and R. Van Deun, "Nano- and micro-sized rare-earth carbonates and their use as precursors and sacrificial templates for the synthesis of new innovative materials," *Chemical Society Reviews*, vol. 44, no. 8, pp. 2032–2059, 2015.

[9] P. Kim, A. Anderko, A. Navrotsky, and R. Riman, "Trends in structure and thermodynamic properties of normal rare earth carbonates and rare earth hydroxycarbonates," *Minerals*, vol. 8, no. 3, p. 106, 2018.

[10] L. Spiridigliozzi, G. Dell'Agli, A. Marocco et al., "Engineered co-precipitation chemistry with ammonium carbonate for scalable synthesis and sintering of improved $Sm_{0.2}Ce_{0.8}O_{1.90}$ and $Gd_{0.16}Pr_{0.04}Ce_{0.8}O_{1.90}$ electrolytes for IT-SOFCs," *Journal of Industrial and Engineering Chemistry*, vol. 59, pp. 17–27, 2018.

[11] J.-G. Li, T. Ikegami, Y. Wang, and T. Mori, "Reactive ceria nanopowders via carbonate precipitation," *Journal of the American Ceramic Society*, vol. 85, no. 9, pp. 2376–2378, 2002.

[12] C. D. Cress, C. S. Redino, B. J. Landi, and R. P. Raffaelle, "Alpha-particle-induced luminescence of rare-earth-doped Y_2O_3 nanophosphors," *Journal of Solid State Chemistry*, vol. 181, no. 8, pp. 2041–2045, 2008.

[13] G. Accardo, L. Spiridigliozzi, R. Cioffi et al., "Gadolinium-doped ceria nanopowders synthesized by urea-based homogeneous co-precipitation (UBHP)," *Materials Chemistry and Physics*, vol. 187, pp. 149–155, 2017.

[14] Z. Guo, F. Jian, and F. Du, "Sonochemical synthesis of luminescent $CeCO_3OH$ one-dimensional quadrangular prisms," *Materials Research Bulletin*, vol. 44, no. 10, pp. 1959–1962, 2009.

[15] Y. Zhang, M. Gao, K. Han, Z. Fang, X. Yin, and Z. Xu, "Synthesis, characterization and formation mechanism of dumbbell-like $YOHCO_3$ and rod-like $Y_2(CO_3)_3{\cdot}2.5H_2O$," *Journal of Alloys and Compounds*, vol. 474, no. 1-2, pp. 598–604, 2009.

[16] G. Dell'Agli, L. Spiridigliozzi, A. Marocco et al., "Morphological and crystalline evolution of Sm-(20 mol%)–doped ceria nanopowders prepared by a combined co-precipitation/hydrothermal synthesis for solid oxide fuel cell applications," *Ceramics International*, vol. 43, no. 15, pp. 12799–12808, 2017.

[17] K. Gao, Y.-Y. Zhu, D.-Q. Tong, L. Tian, Z.-H. Wang, and X.-Z. Wang, "Hydrothermal synthesis of single-crystal $CeCO_3OH$ and their thermal conversion to CeO_2," *Chinese Chemical Letters*, vol. 25, no. 2, pp. 383–386, 2014.

[18] G. Dell'Agli, G. Mascolo, M. C. Mascolo, and C. Pagliuca, "Crystallization-stabilization mechanism of yttria-doped zirconia by hydrothermal treatment of mechanical mixtures of zirconia xerogel and crystalline yttria," *Journal of Crystal Growth*, vol. 280, no. 1-2, pp. 255–265, 2005.

[19] G. Dhanaraj, K. Byrappa, V. Prasad, and M. Dudley, *Handbook of Crystal Growth*, Springer, Berlin Heidelberg, 2010.

[20] K. Nakagawa, Y. Tezuka, T. Ohshima et al., "Formation of cerium carbonate hydroxide and cerium oxide nanostructures by self-assembly of nanoparticles using surfactant template and their catalytic oxidation," *Advanced Powder Technology*, vol. 27, no. 5, pp. 2128–2135, 2016.

[21] C. Sun, J. Sun, G. Xiao et al., "Mesoscale organization of nearly monodisperse flowerlike ceria microspheres," *The Journal of Physical Chemistry B*, vol. 110, no. 27, pp. 13445–13452, 2006.

[22] F. Hrizi, H. Dhaouadi, and F. Touati, "Cerium carbonate hydroxide and ceria micro/nanostructures: synthesis, characterization and electrochemical properties of $CeCO_3OH$," *Ceramics International*, vol. 40, no. 1, pp. 25–30, 2014.

[23] Z. H. Han, N. Guo, K. B. Tang, S. H. Yu, H. Q. Zhao, and Y. T. Qian, "Hydrothermal crystal growth and characterization of cerium hydroxycarbonates," *Journal of Crystal Growth*, vol. 219, no. 3, pp. 315–318, 2000.

[24] B. D. Cullity, *Elements of X-ray Diffraction*, Addison-Wesley Publishing, Boston, MA, USA, 2nd edition, 1978.

[25] H. Toraya, "A new method for quantitative phase analysis using X-ray powder diffraction: direct derivation of weight fractions from observed integrated intensities and chemical compositions of individual phases," *Journal of Applied Crystallography*, vol. 49, no. 5, pp. 1508–1516, 2016.

[26] M. Hirano and E. Kato, "Hydrothermal synthesis of two types of cerium carbonate particles," *Journal of Materials Science Letters*, vol. 18, no. 5, pp. 403–405, 1999.

[27] L. Zhong, K. Li, Y. Luo, M. Li, H. Wang, and G. Li, "Phase evolution of VO_2 polymorphs during hydrothermal treatment in the presence of AOT," *Crystal Growth & Design*, vol. 17, no. 11, pp. 5927–5934, 2017.

[28] G. Dell'Agli, L. Spiridigliozzi, M. Pansini, G. Accardo, S. P. Yoon, and D. Frattini, "Effect of the carbonate environment on morphology and sintering behaviour of variously co-doped (Ca, Sr, Er, Pr) Samarium-doped Ceria in co-precipitation/hydrothermal synthesis," *Ceramics International*, vol. 44, pp. 17935–17944, 2018.

[29] G. Dell'Agli, G. Mascolo, M. C. Mascolo, and C. Pagliuca, "Weakly-agglomerated nanocrystalline $(ZrO_2)_{0.9}(Yb_2O_3)_{0.1}$ powders hydrothermally synthesized at low temperature," *Solid State Science*, vol. 8, no. 9, pp. 1046–1050, 2006.